

# Bu er-gas induced absorption resonances in Rb vapor

Eugeniy E. Mikhailov, Irina Novikova, Yuri V. Rostovtsev, and George R. W. Elch  
 Department of Physics and Institute for Quantum Studies,  
 Texas A & M University, College Station, Texas 77843-4242  
 (Dated: January 22, 2019)

We observe the transformation of the electromagnetically induced transparency (EIT) resonance to absorption in a configuration in a cell filled by  $^{87}\text{Rb}$  and buffer gas. This transformation occurs as the one-photon detuning of the coupling field is varied from resonance. No such absorption resonance is found in the absence of buffer gas. The width of the absorption resonance is several times smaller than the width of the EIT resonance, and its amplitude is about the same. Similar absorption resonances are detected in Hanle configuration in a buffered cell, although the reasons for these effects are quite different.

## I. INTRODUCTION

The coherent interaction of atoms with electromagnetic fields has attracted increasing attention recently in studies of nonlinear and quantum optics as well as spectroscopy and precision metrology. One of the most interesting and versatile effects is coherent population trapping (CPT) [1, 2, 3]. Under the combined action of several resonant laser fields, atoms are optically pumped into a coherent superposition of the ground-state hyperfine or magnetic sublevels which is decoupled from the original electromagnetic fields. That is, the atoms are optically pumped into a so-called "dark" state. Such a medium possesses unique optical properties such as cancellation of absorption (EIT) [4, 5, 6], and steep nonlinear dispersion [4, 7, 8, 9]. The characteristic width of these nonlinear features is determined by the inverse lifetime of an atom in the coherent superposition of ground states. Since radiative transitions are usually forbidden between these states, the coherence can be preserved for a long time, and in atomic cells its lifetime is usually determined by the interaction time of the atom with the laser beams [10, 11].

The addition of a buffer gas (inert gasses,  $\text{N}_2$ ,  $\text{CO}_2$ ,  $\text{CH}_4$ , etc.) to the atomic vapor is a common method for obtaining narrow EIT resonances. Because of the extremely low spin-exchange cross-section, the collisions between rubidium and buffer gas atoms form molecules do not destroy the quantum coherence of the internal states of the atoms, but effectively prolong the time they stay inside the laser beam(s). The processes of decoherence and redistribution of atomic population have been extensively studied in optical pumping experiments [12, 13, 14]. Substantial narrowing of the dark resonance linewidth is reported in [15, 16, 17, 18].

In this paper we experimentally demonstrate that, in the presence of buffer gas, the transmission peaks corresponding to EIT can be transformed into enhanced absorption peaks for proper laser detuning. We observe this effect in two experimental arrangements: in a two-

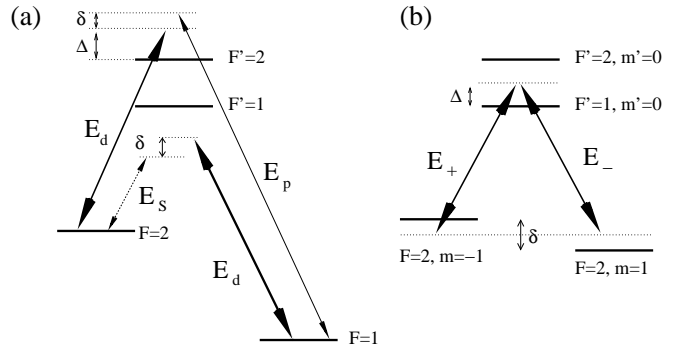


FIG. 1: (a) Three-level interaction scheme of three laser fields with  $^{87}\text{Rb}$  atoms: the long-lived coherence is created on hyperfine ground-state sublevels with strong driving field  $E_d$  and weak probe (anti-Stokes) field  $E_p$ ; the probe and Stokes field  $E_s$  are generated by electro-optic modulation. (b) Hanle configuration: the ground-state coherence is created on magnetic sublevels with two circularly polarized components  $E$  of a monochromatic linearly polarized laser field. In both cases  $\Delta$  is the one-photon detuning of the laser(s) from atomic resonance, and  $\delta$  is the two-photon detuning due to frequency mismatch in case (a) or an external magnetic field in case (b).

level configuration, where strong and weak laser fields form a scheme on two ground-state hyperfine sublevels (Fig. 1a), and in the Hanle configuration (Fig. 1b). It is important to emphasize that in both cases the atoms are prepared in a coherent superposition of levels (hyperfine states in the first case and magnetic sublevels in the latter), and that in both cases no transition to absorption is observed (that is, EIT is preserved) in the absence of buffer gas. A related effect has been reported by Alderbach et al. [19]. In this work the enhanced absorption is observed in a bichromatic standing wave as a result of atomic motion. Because of large Doppler shifts, moving atoms effectively interact with a double-level configuration, which may result in both suppression or enhancement of absorption, depending on the relative phases of the fields. This theory, however, cannot be applied to the present experimental data, since our experiments are carried out with running waves.

The effect reported here is also different from Elec-

from magnetically Induced Absorption (EIA) [20, 21, 22, 23, 24, 25, 26], or the closely related enhanced absorption Hanle effect [7, 28, 29, 30, 31]. In those cases, a narrow peak is observed in the absorption of the probe

eld interacting with a quasi-degenerate two-level system. However, it is a general requirement in both of those cases that the degeneracy of the ground state must be lower than that of the excited state, i.e.  $F < F^0$ . When that requirement is met, the dark state does not exist and narrow EIA resonances are due to the spontaneous coherence transfer from the excited states of the atoms [23, 24, 32]. In addition, the experimental arrangements for traditional EIA experiments involve laser

elds resonant with the corresponding atomic transitions, whereas the narrow absorption resonances discussed in this paper appear for far-detuned laser elds.

This paper is organized as follows. In the next Section we describe the experimental apparatus and measurement technique. In Section III we present the experimental study of these resonances in the three-level scheme based on the hyperfine coherence in atomic cells with different amounts of buffer gas. We then show a theoretical analysis in Section IV. Resonant four-wave mixing and the lineshape of the generated field resonances are discussed in Section V. A brief analysis of the widths of the coherent resonance is given in Section VI. In Section VII, we present the experimental results on the enhanced absorption resonances observed in the Hanle-configuration, together with a qualitative discussion of their origin. A brief summary of the work appears in the final Section.

## II. EXPERIMENTAL SETUP

A schematic of the experimental setup is shown in Fig. 2. An external cavity diode laser is tuned to the  $5S_{1/2} \rightarrow 5P_{1/2}$  ( $D_1$ ) transition of  $^{87}\text{Rb}$ . The probe field (and an additional Stokes field) are produced by an electro-optic modulator (EOM) driven by a stable, narrow-band, microwave generator tuned to the 6.835 GHz ground-state hyperfine frequency. The microwave frequency is adjustable about this frequency, which allows for tuning of the probe field frequency. The probe and Stokes field have equal intensities of approximately 10% of that of the drive field. After the EOM, all

elds pass through a single-mode optical fiber to create a clean spatial mode with a Gaussian intensity distribution and to increase the diameter of the output beam to 7 mm. The fields are circularly polarized with a quarter-wave plate placed after the fiber.

In this experiment we use several glass cells filled with isotopically enhanced  $^{87}\text{Rb}$  and various pressures and types (Ne, Kr) of buffer gas. The cell is placed inside a 3-layer magnetic shield to screen the laboratory magnetic field from the system. The cell is heated to 60°C to increase the density of the  $^{87}\text{Rb}$  vapor to approximately  $2.5 \times 10^{11} \text{ cm}^{-3}$ . After traversing the cell, all three fields are mixed on a fast photodiode with an addi-

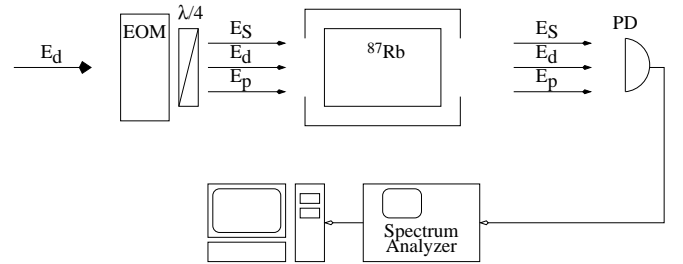


FIG. 2: Schematic of the experimental setup.

tional field shifted by 60 MHz with respect to the driving field. The resulting photo-current is measured with a spectrum analyzer to separate the transmission signals of the probe and Stokes components (see Fig. 2). This detection scheme has been described previously [33, 34].

For our studies in the Hanle configuration, the electro-optical modulator is removed so that there is only one linearly polarized monochromatic electromagnetic field propagating through the cell. The transmitted intensity is recorded directly from a photodetector. A longitudinal magnetic field for shifting the Zeeman sublevels is created by a solenoid mounted inside the inner magnetic shield.

## III. ENHANCED ABSORPTION DUE TO BUFFER GAS IN HYPERFINE SCHEME

In a configuration, the drive field couples the ground-state  $5S_{1/2} F = 2$  level to the excited  $5P_{1/2} F^0 = 2$  level. The probe field couples the ground-state  $5S_{1/2} F = 1$  level to the same excited state. This is shown in Fig. 1a. When both of these fields are on resonance, the atoms are optically pumped into a dark state under the combined action of the strong drive and weak probe, and an EIT resonance is observed in the transmission of the probe field. This is shown in the bottom curves in Fig. 3. Simultaneously, a second scheme is formed with the drive field and the Stokes field that is also generated by the EOM. However this second system is far detuned from both excited levels, so its influence on the ground-state coherence is negligible.

Figure 3 shows that for zero one-photon detuning all EIT resonances are symmetric, which is in agreement with theoretical predictions [35, 36] and our numerical simulations. The main difference between the cells with different amount of buffer gas is the width of the EIT peaks resulting from the increased interaction time as the buffer gas pressure is increased.

The shape of the transmission resonances changes, however, as we tune the lasers from one-photon resonance, and the character of this change depends strongly on the presence of the buffer gas in an atomic cell. If there is no buffer gas present, the EIT peak stays symmetric for all values of . However, the behavior is very different in cells with buffer gas. As the one-photon detuning increases, the EIT resonance becomes asymmetric, and

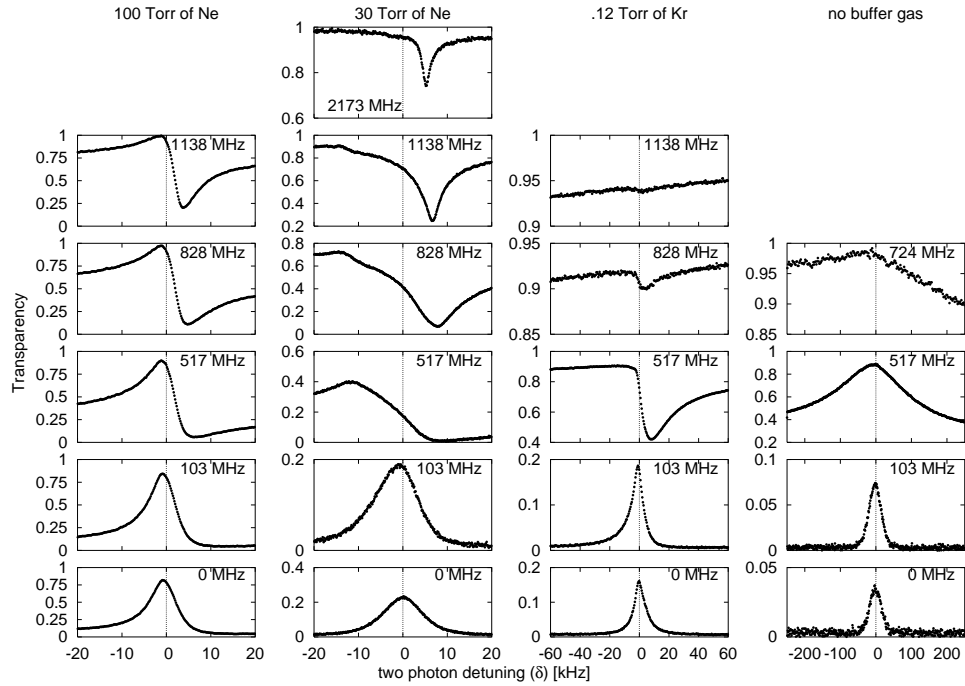


FIG. 3: Transmission of the probe field as a function of two-photon detuning  $\delta$  for various one-photon detunings  $\omega$ . The values of  $\omega$  are shown on the upper right corner of each graph. These data are recorded in the presence of (columns, left to right) 100 Torr of Ne, 30 Torr of Ne, 0.12 Torr of Kr, and no buffer gas. The vertical scale is arbitrary but the same for all graphs. The asymmetry of the resonance curves for  $\omega = 828$  and  $1138$  MHz in the cell with 0.12 Torr Kr, and for  $\omega = 517$  and  $740$  MHz in the vacuum cell are due to the slope of the one-photon absorption contour.

then gradually transforms into a narrow absorption resonance.

Let us emphasize here some of the important properties of these resonances. For example, the cell with 30 Torr of Ne (Fig. 3) shows that the amplitude of the enhanced absorption peak observed for large detuning ( $\omega = 1 \{ 2$  GHz) is comparable to, and sometimes larger than, the amplitude of the EIT peak at  $\omega = 0$ , and its width is narrower. Second, the range of laser detuning for which the absorption resonance is observed ( $> 3$  GHz) is much wider than the linewidth of the one-photon absorption determined by the Doppler width. Thus, the enhanced absorption peaks appears on top of 100% transmission of the probe field.

It is important to note here that the asymmetry in the EIT resonances for nonzero one-photon detuning of the laser fields has been observed by Knappe et al. [7] as well as by Lev et al. [8] in maser emission in the CPT process. However, the modification of the resonance line-shape that they reported is significantly weaker than that reported here. Knappe et al. also suggested an empirical expression for the resonance line-shape, which was later derived theoretically by Taidenachev et al. [9] in the limit of weak interaction fields (perturbation approach). The derivation of this expression for the case of strong laser field is given in the next Section:

$$f(\delta) = \frac{A \sim + B \left( \frac{\omega_0}{\delta} \right)}{\sim^2 + \left( \frac{\omega_0}{\delta} \right)^2} + C \quad (1)$$

Here  $\delta$  is the two-photon detuning,  $\sim$  is the effective width of the coherent resonance, and  $A$ ,  $B$ , and  $C$  are fitting parameters which are functions of the one-photon detuning  $\omega$ . We introduce a shift  $\omega_0$  of the resonance position from the resonant conditions to reproduce the experimental data. One can see that this expression consists of symmetric and anti-symmetric Lorentzian functions of  $\delta$  with amplitudes  $A$  and  $B$  respectively. Parameter  $C$  reflects the absorption of the electromagnetic field, which is determined by incoherent processes.

It is convenient to write the coefficients  $A$  and  $B$  in the following form :

$$A = D \cos(\phi); \quad B = D \sin(\phi); \quad (2)$$

so that the Eq. (1) can be written as:

$$f(\delta) = < D(\phi) e^{i(\phi)} \frac{\sim}{\sim^2 + i(\phi - \omega_0)} + C : \quad (3)$$

In this case, parameter  $D$  characterizes the amplitude of the resonance, and the angle  $\phi$  expresses the ratio between the symmetric and anti-symmetric components in Eq. (1). For example,  $\phi = 0$  represents a symmetric peak of enhanced transmission,  $\phi = \pi$  corresponds to a symmetric peak of enhanced absorption, and  $\phi = \pi/2$  corresponds to a pure dispersion-like lineshape.

These parameters are shown as functions of one-photon detuning in different cells in Figs. 4 and 5. We note that

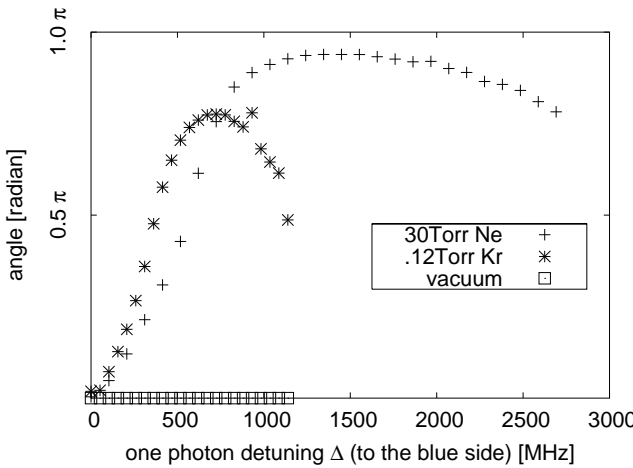


FIG. 4: Angle of two photon resonance for  $^{87}\text{Rb}$  cells with different amount of a buffer gas.

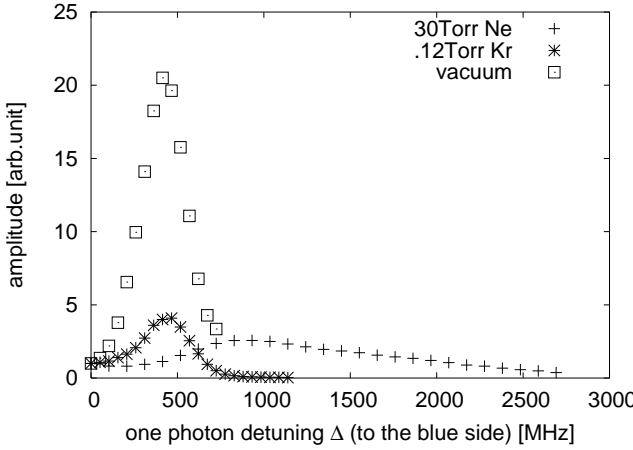


FIG. 5: Amplitude of the two-photon resonance. For easier comparison, the values of  $D$  are normalized to the resonance amplitude at zero detuning.

no deviation from the Lorentzian form is observed for the EIT resonance in a vacuum cell ( $\gamma = 0$  for all detunings). However, buffered cells show the change from a symmetric transmission resonance (for  $\gamma = 0$ ) to almost symmetric absorption resonance for  $\sim 700$  MHz for 0.12 Torr buffer gas pressure and  $\sim 1.4$  GHz for 30 Torr buffer gas pressure. Note that the highest "angle" is achieved in the cell with largest amount of the buffer gas. After reaching its maximum, the angle starts to decline again, although we never observe the recovery of the symmetric EIT peak for larger detunings.

#### IV. THEORETICAL ANALYSIS

We now derive an expression for the absorption coefficient of a weak probe field in a closed three-level scheme as shown in Fig. 6. In this case, the time-

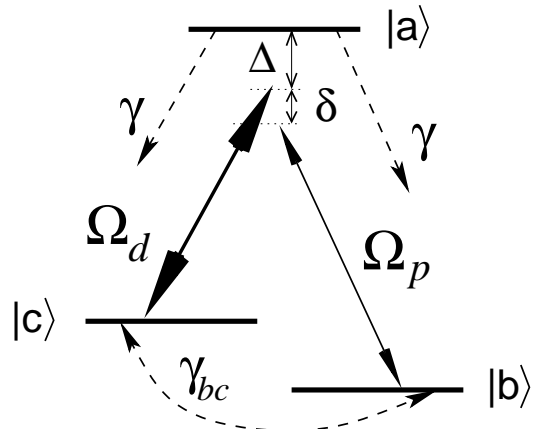


FIG. 6: Three-level system.

evolution equations for the density matrix elements are the following (see, e.g. [36]):

$$\dot{\rho}_{bb} = i_{p,ab} \rho_{pb} - i_{p,ba} \rho_{ab} + r_{aa} \rho_{bb} - \gamma_{bc} \rho_{bb} + \gamma_{cc} \rho_{cc} \quad (4)$$

$$\dot{\rho}_{cc} = i_{d,ac} \rho_{dc} - i_{d,ca} \rho_{ca} + r_{aa} \rho_{cc} - \gamma_{bc} \rho_{cc} + \gamma_{bb} \rho_{bb} \quad (5)$$

$$\dot{\rho}_{ab} = i_{p,ab} \rho_{ab} + i_{p,ba} (\rho_{bb} - \rho_{aa}) + i_{d,cb} \rho_{cb} \quad (6)$$

$$\dot{\rho}_{ca} = i_{d,ac} (\rho_{ca} - \rho_{aa}) - i_{p,ab} \rho_{ab} \quad (7)$$

$$\dot{\rho}_{cb} = i_{p,cb} \rho_{cb} - i_{d,ca} \rho_{ca} \quad (8)$$

where  $i_d = \gamma_{ac} E_p \sim$  and  $i_p = \gamma_{ab} E_d \sim$  are the Rabi frequencies of the drive and probe fields. The generalized decay rates are defined as:

$$\gamma_{ab} = r + i_d (\gamma_r + \gamma_{\text{deph}}); \quad (9)$$

$$\gamma_{ac} = r + i_d; \quad (10)$$

$$\gamma_{cb} = \gamma_{bc} + i_d; \quad (11)$$

Here  $\gamma_r = r + \gamma_{\text{deph}}$  is the polarization decay rate,  $r$  is the radiative decay rate of the excited state,  $\gamma_{\text{deph}}$  is the dephasing rate of the optical transition due to non-radiative effects, and  $\gamma_{bc}$  is the inverse lifetime of the coherence between ground states  $|j_1\rangle$  and  $|j_2\rangle$ . The presence of the buffer gas affects values of both  $\gamma_{bc}$  and  $r$ . On one hand, as mentioned above, it allows for a longer ground-state coherence lifetime. On the other hand it broadens the optical transition, since  $\gamma_{\text{deph}}$  grows linearly with buffer gas pressure [40].

Solving these equations in the steady state regime and assuming  $j_{1,p} = j_{1,d}$  we obtain the following expression for the linear susceptibility of the probe field:

$$= \frac{\gamma_{ab} (\rho_{aa}^{(0)} - \rho_{bb}^{(0)}) + \frac{j_d j_p^2}{c\lambda} (\rho_{aa}^{(0)} - \rho_{cc}^{(0)})}{\gamma_{ab} \gamma_{cb} + \frac{j_d j_p^2}{c\lambda}}; \quad (12)$$

Where  $\gamma = \frac{3}{8} N^2 r$ ,  $N$  is the  $^{87}\text{Rb}$  density and  $\lambda$  is the wavelength of the probe field.

The atomic population differences in the approxim a-

tion of strong driving field ( $j_{d\beta}$ ) and  $j_{bc}$ ) are:

$$\left( \begin{array}{cc} (0) & (0) \\ aa & bb \end{array} \right), \quad \frac{bc}{2} \frac{j_{d\beta}^2}{bc^2 + j_{d\beta}^2} \quad (13)$$

$$\left( \begin{array}{cc} (0) & (0) \\ aa & cc \end{array} \right), \quad \frac{bc}{2} \frac{(j_{d\beta}^2 + j_{bc}^2)}{bc^2 + j_{d\beta}^2} : \quad (14)$$

By substituting these expressions into Eq. (12), we find the absorption coefficient as a function of two-photon detuning:

$$= \frac{bc}{2} \frac{j_{d\beta}^2}{2} \frac{bc j_{d\beta}^2 + j_{bc}^2}{bc^2 + (j_0)^2} ; \quad (15)$$

where

$$j_0 = j_{d\beta} \frac{2}{2 + 2} \quad (16)$$

is the ac-Stark shift of the excited state, and

$$= \frac{p}{2} \frac{j_{d\beta}^2 + \frac{2}{bc} (j_{d\beta}^2 + j_{bc}^2)}{2 + 2} \quad (17)$$

is the effective width of the two-photon transmission resonance.

Using Eq. (15) for the absorption coefficient we can now find expressions for the coefficients  $A$ ,  $B$ , and  $C$  in Eq. (1) which describe the line-shape of the two-photon resonance for the probe field propagating through a medium of length  $L$ . For the moment we restrict ourselves to the case of optically thin media, so  $I_{out} = I_{in} e^{-I_{in} (1 - L)}$ :

$$A = L \frac{j_{d\beta}^2}{2 + 2} \frac{j_{d\beta}^2 (j_{d\beta}^2 + j_{bc}^2)}{2 j_{d\beta}^2 + \frac{2}{bc} (j_{d\beta}^2 + j_{bc}^2)^2} \quad (18)$$

$$B = L \frac{j_{d\beta}^2}{2 + 2} \quad (19)$$

$$C = 1 - L \frac{j_{d\beta}^2}{2 + 2} \quad (20)$$

$$= \frac{bc}{2} \frac{j_{d\beta}^2}{bc^2 + j_{d\beta}^2} : \quad (21)$$

It is easy to see that the coefficient  $C$ , which is determined by incoherent absorption processes in this approximation, coincides with the absorption of a weak field in a two-level scheme. The only difference is the coefficient which represents the redistribution of the atomic population between ground levels:  $p = 1$  when the one-photon detuning is small ( $j_{d\beta} = j_{bc}$ ) means all atomic population is optically pumped into a dark state, and  $p = 1/2$  if the laser is far-detuned, and the populations of the levels  $j_{bi}$  and  $j_{ci}$  are almost the same.

Coefficient  $A$  is a symmetric function of the one-photon detuning. Its sign changes as  $j_{d\beta}$  gets larger:  $A$  is positive for small detunings, then at  $j_{d\beta}^2 = j_{bc}^2$  it disappears, and for larger the amplitude of the symmetric component of the resonance becomes negative (i.e.

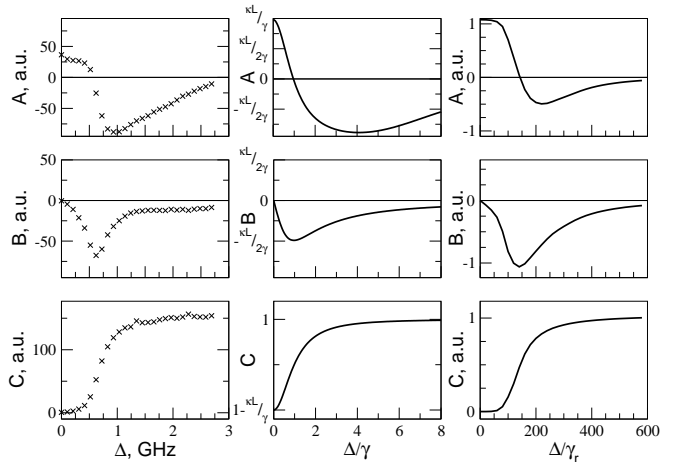


FIG. 7: Coefficients  $A$ ,  $B$ , and  $C$  describing the line-shape of the coherent resonance Eq. (1): extracted from the experimental data for  $^{87}\text{Rb}$  cell with 30 Torr (left column), calculated using Eqs. (18-20) (middle column), and obtained by numerical modelling (right column).

absorptive). Coefficient  $B$  is an odd function of  $\Delta$ , and exactly zero on resonance.

Thus it is clear why there is no distortion of the symmetric Lorentzian line-shape observed for the cell without buffer gas. In this case the inhomogeneous broadening of the transitions is much larger than the radiative decay rate of the excited state, so the resulting shape of the EIT resonance should be an average over the Doppler distribution. This means that the anti-symmetric part of Eq. (1) effectively cancels. At the same time, the simplified theoretical model described above should also be applicable for the case of high buffer gas pressure, for which the collisional broadening of the excited state exceeds the Doppler broadening.

A comparison of coefficients  $A$ ,  $B$ , and  $C$  given by Eqs. (18-20), with those obtained by fitting our experimental data for the Rb cell with 30 Torr of Ne is shown in Fig. 7. One can immediately see that the theoretical formulae qualitatively describe the dependence of the coefficients as functions of one-photon detuning, although they are not accurate enough for a quantitative analysis. There are several reasons for this. On one hand, the collisional broadening created by a Ne pressure of 30 Torr is still smaller than the Doppler broadening, so that averaging over the velocity distribution can still significantly affect the shape of the resonance. Further, we assumed for simplicity that the medium is optically thin and there is no absorption of the drive field which is not the case for the experimental conditions. One of the consequences of this effect is the density narrowing of the coherent resonances which will be discussed in the following Section.

To analyze the effects of propagation through the optically thick medium and thermal velocity distribution of the Rb atoms, we perform a numerical simulation of the interaction of the drive and probe field with the three-

level system considered above. In this case we take into the account the attenuation of the probe intensity as the fields propagate through the optically thick medium. In addition, since atoms with different velocities "see" the electromagnetic fields at a shifted frequency, the real susceptibility has to be averaged over the Maxwell velocity distribution:

$$\langle \rangle = \frac{1}{P} \int_{-ku}^{Z+1} \langle \rangle (kv) e^{-\frac{(kv)^2}{(ku)^2}} d(kv); \quad (22)$$

where  $k = d/c$  is the drive field wave-vector, and  $u = \sqrt{2k_B T/M}$  is the most probable thermal speed (here  $T$  is the temperature of the vapor,  $M$  is the mass of Rb atom and  $k_B$  is the Boltzmann constant). In general, this problem is straightforward but extremely cumbersome and can be solved only numerically.

To best model the experimental data obtained in the Rb cell with 30 Torr of Ne we use following parameters:  $d_{\text{ph}} = 10 \text{ cm}$ ,  $b_c = 5 \times 10^4 \text{ cm}^{-1}$ ,  $ku = 50 \text{ cm}^{-1}$ ,  $d = 0.4 \text{ cm}$ , and  $p = 0.1 \text{ cm}^3$ . The values of Rabi frequencies for the actual fields are  $d = 0.38 \text{ cm}^{-1}$  ( $I_d = 1.2 \text{ mW/cm}^2$ ) and  $p = 0.13 \text{ cm}^3$  ( $I_d = 0.13 \text{ mW/cm}^2$ ). The small deviation between these values can be attributed to the nonuniform spatial distribution of the laser intensity. For the vacuum cell, all the same parameters are used except for the value of  $b_c = 10^2 \text{ cm}^{-1}$  and  $d_{\text{ph}} = 0$ .

The results of the numerical simulation are shown in Fig. 7c. Although they do not exactly coincide with the experimental data, they allow better understanding of why no absorption resonances are observed in the cell with no buffer gas. The calculated values of the resonance amplitude  $D$  and the ratio  $\langle \rangle$  are shown in Figs. 8 and 9. These shows that the inversion of the EIT resonance occurs in the cell with buffer gas, whereas in the cell without buffer gas no absorption resonances ever appear. However, these calculations show that noticeable asymmetry of the resonance is expected for values of laser detuning ( $|\Delta| > 100 \text{ cm}^{-1}$ ), for which the amplitude of the resonances is very small and hardly detectable.

The importance of Doppler averaging is also observed in the two-photon resonance shift  $\Delta_0$ . It is easy to see in Fig. 3 that for non-zero detuning  $\Delta$  the centers of both EIT and buffer-gas induced absorption resonances are shifted from zero two-photon detuning. One of the reasons for this effect is the light shift of the atomic levels, as shown by Eq. (16). However, this dependence on the laser detuning differs significantly from the behavior of the resonance shift measured experimentally (Fig. 10). A more realistic resonance shift as a function of laser detuning is obtained by numerical simulation if Doppler averaging is performed (Fig. 10, inset).

We note that both the prediction of the theoretical model and the result of the numerical simulation developed above are for a three-level system, and provide only qualitative agreement with the experimental results. There are several important effects which are not considered here. For example, neither hyperfine structure of the excited state nor Zeeman substructure of all states is taken

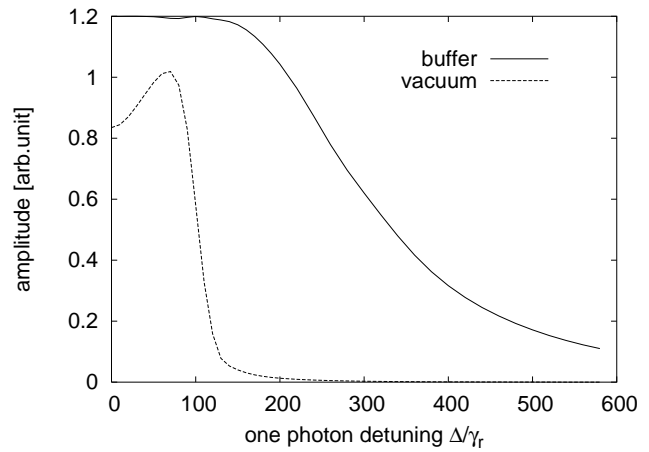


FIG. 8: Numerical calculation of the resonance strength  $\langle \rangle$  vs one-photon detuning for a probe field propagating in a medium with buffer gas and vacuum. One-photon detuning and resonance width are given in units of  $\text{cm}^{-1}$ .

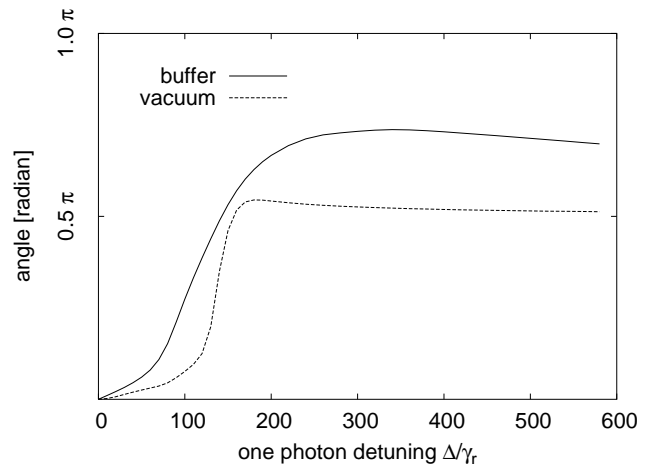


FIG. 9: Numerical calculation of angle  $\langle \rangle$  vs one-photon detuning for a probe field propagating in a medium with buffer gas and vacuum. One-photon detuning and resonance width are given in units of  $\text{cm}^{-1}$ .

into consideration, although it may have a profound effect on the coherent interaction. In addition, no influence of four-wave mixing processes and the generation of a Stokes field is taken into account.

We numerically compare the case of large detuning ( $|\Delta| = 250 \text{ cm}^{-1}$ ) for the case of cells with buffer and vacuum for various drive power values ( $I_d$ ). This shows that the absorption resonance appears only for large enough drive laser power in the cell with buffer gas, whereas in the cell without buffer gas the resonance remains dispersion-like ( $\langle \rangle = 2$ ).

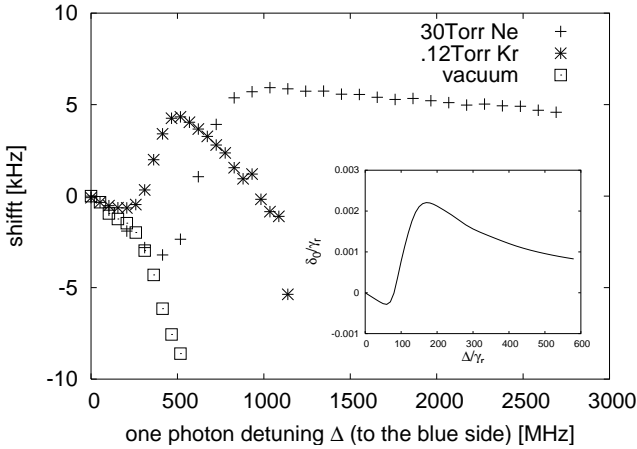


FIG. 10: Two photon resonance shift ( $\delta$ ) as a function of one-photon detuning for the vacuum cell (squares), cell with 0.12 Torr of Kr (stars) and with 30 Torr of Ne (crosses). Inset: the result of the numerical simulation for the 30 Torr cell.

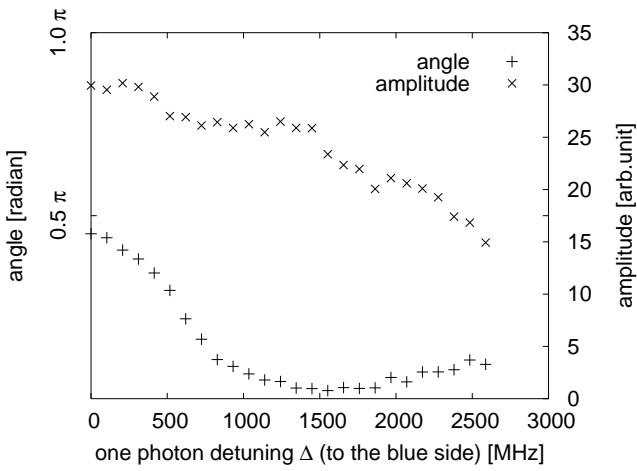


FIG. 11: Angle ( $\delta$ ) and amplitude ( $D$ ) of the two photon resonance for the generated Stokes field.

## V. INFLUENCE OF THE BUFFER GAS ON FOUR-WAVE MIXING

Many previous publications [33, 41, 42, 43] have shown that dense coherent media contribute to significant enhancement of nonlinear processes. In particular, under the conditions of our experiment this leads to strong four-wave mixing: the drive field applied to the  $F = 1$  level, is scattered by the ground-state coherence, which leads to the generation of a coherent Stokes field. This process does not require the presence of a seed field, and is initiated by spontaneous photons [34].

The amplitude and the angle for the generated Stokes field in the cell with 30 Torr of Ne are shown in Fig. 11. One can see that the shape of this resonance also changes as the laser is detuned from the atomic transition: at resonance, the new field has a dispersion-like form (

0.5), and is transformed into a symmetric transmission peak ( $\delta = 0$ ) as  $\delta$  increases.

## VI. WIDTH OF THE PROBE AND STOKES RESONANCES

Narrow resonances with good signal-to-noise ratio are important for many applications. For example, narrow EIT resonances are used for precision metrology [16, 44, 45] and atomic clocks [46, 47]. Our experiments demonstrate that the coherent absorption resonances, observed for the far-detuned system, may have more attractive characteristics in terms of the resonance width and amplitude than the EIT resonances observed for the zero detuning. For example, in the cell with 30 Torr of Ne the amplitude of the absorption resonance for  $\delta = 1.2$  (2 GHz) is larger than that of the EIT resonance, while its width is narrower (for example,  $\sim(0) = \sim(2\text{ GHz}) = 3.3$ ).

The measured widths of the two-photon resonance as functions of the one-photon detuning are shown in Fig. 12 for cells with different buffer gas pressure. Again we see the difference between cells with and without buffer gas: in the latter case the width of the EIT resonance increases significantly with one-photon detuning. However, for the buffered cells the width increases only near atomic resonance, but for larger detuning the resonance width actually decreases with one-photon detuning.

The numerical simulations do not show this. This can be seen in Fig. 13 which shows no strong difference between cells with or without buffer gas. We attribute this to the same shortcomings previously discussed. Even in the vacuum cell there should be a narrowing of the resonance; however, the simulations show that this occurs for large detuning with extremely low resonance amplitudes (compare with Fig. 8).

To study the behavior of the resonance width we will use the theoretical expression for the width of the two-photon resonance Eq. (17) obtained in Section IV. According to that equation, in the strong laser field limit ( $j_d j_{bc} \gg 1$ ) the width of the EIT resonance for small  $\delta$  does not depend on the ground-state coherence decay rate and is determined by power broadening:  $\sim j_d j_{bc}^{-1}$ , as in previous studies [35]. Then the resonance width decreases with one-photon detuning, and for  $j_d j_{bc} \ll 1$  it drops as  $1 = \delta^2$ . Ultimately for  $j_d j_{bc} = 1$ , the width of the resonance is determined by the coherence decay rate  $\gamma_{bc}$ .

We would like to point out two effects that limit the accuracy of this analysis. First, we have not taken into account the velocity distribution of the thermal Rb atoms. Second, propagation through the Rb vapor becomes important for optically thick media. In this case the shape of the coherent resonance may change; in particular, its width can be greatly reduced. This effect is known as density narrowing of the EIT resonances [48, 49].

We note that both the above effects are not very im-

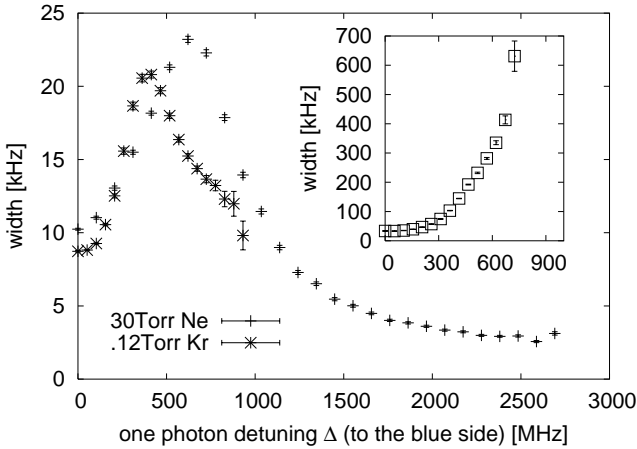


FIG. 12: Width of the two photon resonance  $\sim$  as a function of one-photon detuning for  $^{87}\text{Rb}$  cell with 30 Torr of Ne (cross), 0.12 Torr of Kr (x), and without buffer gas (squares, inset). The minimum width of the EIT resonance in the vacuum cell with no buffer gas is  $\sim (\Delta = 0) = 17$  kHz.

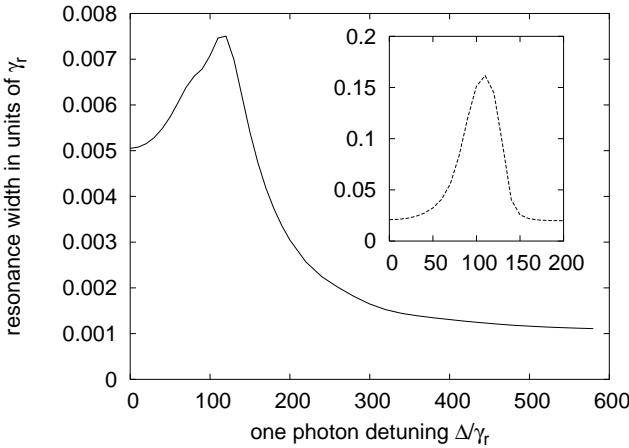


FIG. 13: Numerical calculation of resonance width ( $\sim$ ) vs one-photon detuning for a probe field propagating in a medium with buffer gas and vacuum (inset).

tant when the lasers are far-detuned ( $\Delta \gg \gamma_r$ ) since the absorption of the medium is small, and the parameters describing the resonance lineshape do not change noticeably within the Doppler contour. Thus, for large detuning the dependence of the resonance width predicted from Eq. (17) is in good agreement with the experimental points, as shown in Fig. 14.

To study how the resonance width behaves as a function of one-photon detuning for small  $\Delta$  we should take both propagation and Doppler averaging into account. Since it is virtually impossible to do that exactly, we make a few simplifying assumptions that allow us to roughly predict the dependence of the resonance width on the one-photon detuning. First, we assume that the main contribution to the resonance lineshape is due to the resonant velocity subgroup for which  $\text{kv}' = 0$ .

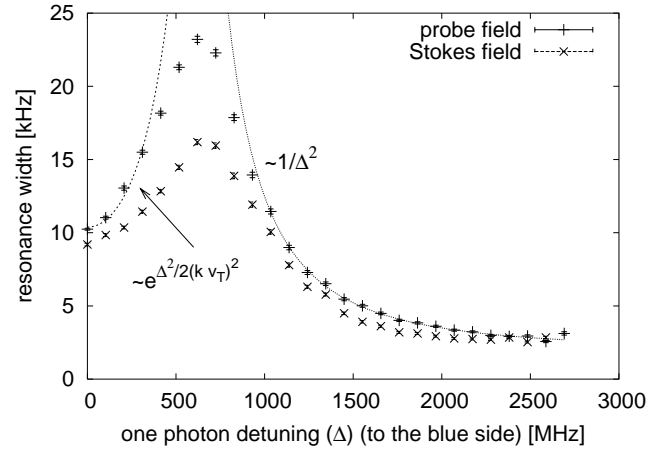


FIG. 14: Width of the two photon resonance ( $\sim$ ) for the probe and generated Stokes field.

Then, the only consequence of the detuning the laser is the reduction of the number of atoms in this velocity group:

$$N(\Delta) / N_0 e^{-\frac{\Delta^2}{(kv_T)^2}} : \quad (23)$$

The output intensity  $I_{\text{out}}$  is then given by

$$I_{\text{out}} / I_{\text{in}} e^{-\frac{L}{j_d j^2} \frac{bc}{j_d j^4}} e^{-\frac{L}{j_d j^2}} : \quad (24)$$

In this expression the first term represents the residual absorption under EIT conditions, and the second one describes the shape of the peak as a function of two-photon detuning. It is easy to see that the width of the resonance in this case is inversely proportional to the atom density [48]:

$$\sim_D(N) / \frac{j_d j^2}{P} \frac{3}{8} N^2 L^{1/2} : \quad (25)$$

We use the expression for the density of the resonant velocity subgroup as a function of laser detuning given by Eq. (23) to obtain the width of the resonance:

$$\sim_D(\Delta) / \frac{j_d j^2}{P} \frac{1}{N L} e^{-\frac{\Delta^2}{(kv_T)^2}} : \quad (26)$$

Fig. 14 shows that this formula works only for a small frequency region in the vicinity of one-photon resonance where the resonance is nearly symmetric and deviates for larger  $\Delta$ . This is consistent with the assumptions made in the derivation.

The width of the Stokes field resonance is also shown in Fig. 14. It has approximately the same shape as the curve for the probe field, but it is worth mentioning that its width can be narrower than that of the probe field while having a similar resonance amplitude.

## VII. ENHANCED ABSORPTION DUE TO ZEEMAN COHERENCE

Let us now consider another kind of coherence effect originating from coherent population trapping, namely nonlinear magneto-optical rotation. A review of this effect is given in Ref. [50]. In this case, the long-lived coherence is created among ground-state Zeeman sublevels by a single electromagnetic field (in general elliptically polarized but usually taken as linear in most experiments and analyses) where the link(s) are formed by the two opposite circularly polarized components  $E$  of the input field (Fig. 1b). In this configuration the transmission is very sensitive to the applied magnetic field, which shifts sublevels with different magnetic quantum number  $m$ . An applied magnetic field  $B$  therefore creates a two-photon detuning proportional to the magnetic field:  $\delta = aB$ , where  $a = 2B_B \approx$  and  $B_B$  is the Bohr magneton. In particular, the polarization of the incident laser field is changed dramatically as a result of the steep dispersion associated with CPT [51, 52]. This effect, known as the nonlinear Faraday effect, or nonlinear magneto-optical polarization rotation, has been extensively studied over the last decades in various experimental configurations: in atomic beams [53, 54], and in glass cells with or without anti-relaxation coating [51, 52, 55, 56, 57, 58, 59, 60, 61].

There are a number of publications which reveal the strong influence of buffer gas on Zeeman coherence. This influence results in significant modifications of the amplitude and lineshape of polarization rotation and EIT resonances [62, 63]. Here we demonstrate that the presence of buffer gas leads not only to the deterioration of EIT but can also lead to narrow enhanced absorption peaks for buffer gas pressure higher than 3 Torr. A detailed analysis of the effect of buffer gas on polarization rotation will be published elsewhere.

The transmission spectrum of  $^{87}\text{Rb}$   $5S_{1/2} F = 2 \rightarrow 5P_{1/2} F' = 1/2$  consists of two transitions, partially resolved within the Doppler contour [52]. Zeeman coherence can be created on both transitions so that linear absorption is suppressed for a linearly polarized electromagnetic field even if the laser frequency differs somewhat from the exact atomic transition frequency. For example, if the laser is tuned exactly between the two transitions ( $\delta = 406 \text{ MHz}$ ), the transmission is still enhanced by 40%.

This is true, however, only if there is no buffer gas present in the cell. The transmission spectra for different pressures of Ne buffer gas are shown in Fig. 15a, b, and c. One can easily see that the effect of CPT decreases with increasing buffer gas pressure. Moreover, the enhanced absorption appears for the frequency region directly between the two transitions. Note, that this effect is clearly due to the ground-state coherence, since if the magnetic field is varied, narrow absorption resonances are detected as shown in Fig. 15d, e, and f.

Here we should emphasize that the reason for the en-

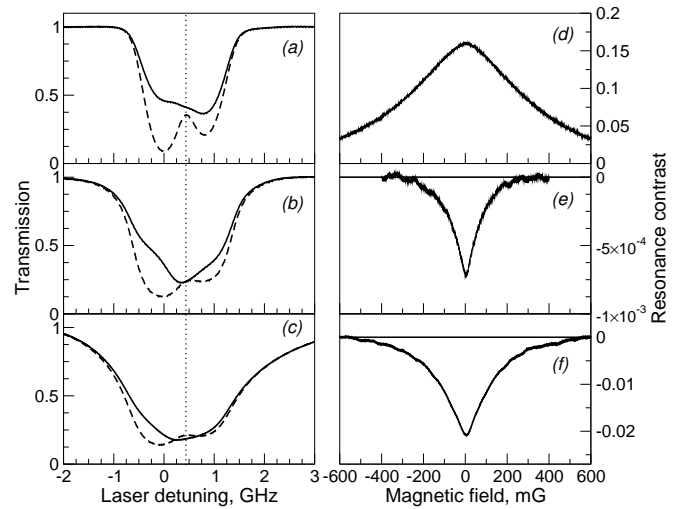


FIG. 15: Left column: transmission through the  $^{87}\text{Rb}$  cells with (a) 1 Torr; (b) 3 Torr; (c) 10 Torr of Ne buffer gas as the laser frequency is swept across the  $F = 2 \rightarrow F' = 1$  transitions. Solid line: transmission at zero magnetic field. In this case the ground state coherence is unperturbed and we denote the transmission as  $T_{\text{coh}}$ . Dashed line: transmission at large magnetic field ( $B \gg B_B$ ). In this case the coherence is destroyed, and we denote the transmission as  $T_{\text{lin}}$ . Right column: The peak contrast in transmission as a function of magnetic field (two-photon detuning) for fixed laser frequency (shown as a dotted line on the previous graphs) for the same cells. The normalization of the output signal is  $C = (T_{\text{coh}} - T_{\text{lin}})/T_{\text{coh}}$ . Thus  $C > 0$  is a manifestation of EIT shown in part (d), and  $C < 0$  indicates enhanced absorption as seen in (e) and (f). Because of the difference in geometrical sizes of the cells, the atomic density is adjusted for each case so that  $T_{\text{lin}} = 80\%$ . Laser power is 2 mW.

hanced absorption resonances described in this Section is quite different from the effects described in the previous sections, despite of their similarities (both effects are observed only in buffered Rb cells and for nonzero one-photon detunings). In the case of Zeeman coherence, the nonlinear enhanced absorption may be explained by the interplay of the matrix elements of the transitions involved in the links. As the laser frequency changes, dark states can be created for both  $F = 2 \rightarrow F' = 1$  and  $F = 2 \rightarrow F' = 2$  transitions. However, because of the difference in relative sign in the transition matrix elements [40], these dark states are orthogonal:

$$D_{i_2, 1} = \frac{1}{2} (j_m = 1i + j_m = -1i); \quad (27)$$

$$D_{i_2, 2} = \frac{1}{2} (j_m = 1i - j_m = -1i); \quad (28)$$

Strictly speaking, because of this difference perfect CPT is not possible in this double-system. However, the natural width of both transitions ( $\delta = 5 \text{ MHz}$ ) is much smaller than their hyperfine splitting, so that when the laser is resonant with one transition, the disturbance introduced by the other transition may be neglected. For

the cell without buffer gas or anti-relaxation coating, atoms do not change their velocity during the interaction process so we observe two Gaussian-shaped transmission peaks as the laser frequency is swept across the  $F = 2 \downarrow F^0$  transitions.

In the presence of buffer gas, the velocity-changing collisions result in a quite different situation. Since the hyperfine structure of the excited level is not completely resolved under Doppler broadening, there is a finite probability that an atom may be optically pumped into the dark state on one transition, and then undergo a velocity changing collision that makes it resonant with the other transition. Because of the difference in sign, the dark state, created on one transition corresponds to the bright state of the other one, so such an atom can absorb light more strongly than one without coherence. Thus, for the symmetric scheme as shown in Fig. 1b, we would expect complete destruction of coherence if the laser is tuned exactly between atomic transitions, so that the probabilities of an atom interacting with either of these transitions are equal. In reality, however, the  $F = 2 \downarrow F^0 = 1$  transition is slightly stronger than the  $F = 2 \downarrow F^0 = 2$  transition, and this imbalance results in the enhanced absorption for a small region of laser frequencies.

### V III. SUMMARY

We demonstrate significant changes of the EIT resonance lineshape in a medium with buffer gas. We show that the shape changes from transparency-like to a dispersion-like and then to absorption-like shape with increasing one-photon detuning. We also show that for large enough detuning, the resonance width is limited by the ground level coherence decay rate ( $\gamma_{bc}$ ). We have

also demonstrated that there is a region of one-photon detunings with larger signal than for zero one-photon detuning, while the width of the resonance is narrower. Observation of this absorption-like resonance is power dependent and takes place only for high enough drive power. We have developed a simple theory that qualitatively describes the observations, and shown the result of numerical simulations that more closely match the experimental observations, and we have accounted for the origin of the discrepancies between these and the data. We compared the behavior of the probe and Stokes field for large one-photon detuning, and showed that the resonance width of these two fields behaves similarly, while the shapes of the resonances are different.

We have also shown that an induced absorption resonance appears with one-photon detuning in the Hanle configuration, although it has a very different origin from that of the bichromatic field case. In this configuration, the enhanced absorption results from the possibility of velocity changing collisions to cause an atom in a dark state on one transition to change to a bright state of another.

The effects reported here differ from previously observed Electromagnetically Induced Absorption resonances and the absorption Hanle effect. Both of those cases have strict requirements on selection rules that are not required or met for our observations.

### IX. ACKNOWLEDGMENTS

We thank A. Zhang, V. A. Sautenkov, A. B. Matsko, and M. O. Scully for the useful and stimulating discussions, and Office of Naval Research for financial support.

---

[1] E. Arimondo and G. Orriols, *Nuovo Cimento Lett.* **17**, 333 (1976).

[2] B. D. Agap'yev, M. B. Gomiy, B. G. Matysov, and Y. V. Rozhdestvenskii, *Usp. Fiz. Nauk* **163**, 1 (1993).

[3] E. Arimondo, *Progress in Optics XXXV*, 259 (1996).

[4] M. O. Scully and M. S. Zubairy, *Quantum Optics* (Cambridge University Press, Cambridge, UK, 1997).

[5] S. E. Harris, *Phys. Today* **50**, 36 (1997).

[6] J. P. Marangos, *J. Mod. Opt.* **45**, 471 (1998).

[7] S. E. Harris, J. E. Field, and A. Kasapi, *Phys. Rev. A* **46**, R29 (1992).

[8] O. Schmidt, R. Wynands, Z. Hussein, and D. Meschede, *Phys. Rev. A* **53**, R27 (1996).

[9] F. Renzoni and E. Arimondo, *Opt. Commun.* **178**, 345 (2000).

[10] E. Arimondo, *Phys. Rev. A* **54**, 2216 (1996).

[11] M. G. Raaf, E. Arimondo, E. S. Fry, D. E. Nikonov, G. G. Padmanabhan, M. O. Scully, and S. Y. Zhu, *Phys. Rev. A* **51**, 4030 (1995).

[12] R. Bernheim, *Optical Pumping* (W. A. Benjamin, Inc., New York, 1965).

[13] J. Vanier, A. Godone, and F. Levi, *Phys. Rev. A* **58**, 2345 (1998).

[14] W. Happer, *Rev. Mod. Phys.* **44**, 169 (1972).

[15] S. Brandt, A. Nagel, R. Wynands, and D. Meschede, *Phys. Rev. A* **56**, R1063 (1997).

[16] R. Wynands and A. Nagel, *Appl. Phys. B* **68**, 1 (1998).

[17] M. Erhard, S. Numann, and H. Helm, *Phys. Rev. A* **62**, 061802(R) (2000).

[18] M. Erhard and H. Helm, *Phys. Rev. A* **63**, 043813 (2001).

[19] C. A. olderbach, S. Knappe, R. Wynands, A. V. Taichenachev, and V. I. Yudin, *Phys. Rev. A* **65**, 043810 (2002).

[20] A. M. Akulshin, S. Barreiro, and A. Lezama, *Phys. Rev. A* **57**, 2996 (1998).

[21] A. Lezama, S. Barreiro, and A. M. Akulshin, *Phys. Rev. A* **59**, 4732 (1999).

[22] A. Lipschitz, S. Barreiro, A. M. Akulshin, and A. Lezama, *Phys. Rev. A* **61**, 053803 (2000).

[23] A. V. Taichenachev, A. M. Tumarkin, and V. I. Yudin, *JETP Lett.* **69**, 819 (1999).

[24] A. V. Taichenachev, A. M. Tumarkin, and V. I. Yudin,

Phys. Rev. A 61, 011802 (2000).

[25] M. Kwon, K. Kim, H. S. Moon, H. D. Park, and J. B. Kim, J. Phys. B 34, 2951 (2001).

[26] C. Y. Ye, Y. V. Rostovtsev, A. S. Zibrov, and Y. M. Golubev, Opt. Comm. 207, 227 (2002).

[27] Y. Dancheva, G. A. Izetta, S. Cartaleva, M. Taslakov, and C. Andreeva, Opt. Comm. 178, 103 (2000).

[28] G. A. Izetta, S. Cartaleva, Y. Dancheva, C. Andreeva, S. Gozzini, L. Botti, and A. Rossi, J. of Opt. B 3, 181 (2001).

[29] F. Renzoni, C. Zimmermann, P. Verkerk, and E. Arimondo, J. Opt. B 3, S7 (2001).

[30] F. Renzoni, S. Cartaleva, G. A. Izetta, and E. Arimondo, Phys. Rev. A 63, 065401 (2001).

[31] C. Andreeva, S. Cartaleva, Y. Dancheva, V. Biancalana, A. Burchianti, C. M. Marinelli, E. M. Ariotti, L. Mori, and K. Nasayrov, Phys. Rev. A 66, 012502 (2002).

[32] H. Failache, P. Valente, G. Ban, V. Lorent, and A. Lezama, Phys. Rev. A 67, 043810 (2003).

[33] M. M. Kash, V. A. Sautenkov, A. S. Zibrov, L. Hollberg, G. R. Welch, M. D. Lukin, Y. Rostovtsev, E. S. Fry, and M. O. Scully, Phys. Rev. Lett. 82, 5229 (1999).

[34] E. E. M. Ikhailov, Y. Rostovtsev, and G. R. Welch, Journal of Modern Optics 49, 2535 (2002).

[35] A. Javan, O. Koccharovskaya, H. Lee, and M. O. Scully, Phys. Rev. A 66, 013805 (2002).

[36] H. Lee, Y. Rostovtsev, C. J. Bednar, and A. Javan, Appl. Phys. B 76, 33 (2003).

[37] S. Knappe, M. Stahler, C. A. olderbach, A. Taichenachev, V. Yudin, and R. Wynands, Appl. Phys. B 76, 57 (2003).

[38] F. Levi, A. G. odone, J. V. ans S. M. icalizio, and G. M. odugno, Eur. Phys. J. D 12, 53 (2000).

[39] A. V. Taichenachev, V. I. Yudin, R. Wynands, M. Stahler, J. Kitching, and L. Hollberg, Phys. Rev. A 67, 033810 (2003).

[40] J. Vanier and C. Audoin, The Quantum Physics of Atomic Frequency Standards, vol. 1 (Adam Hilger, Philadelphia, 1989).

[41] M. D. Lukin, M. Fleischhauer, A. S. Zibrov, H. G. Robinson, V. L. Velichansky, L. Hollberg, and M. O. Scully, Phys. Rev. Lett. 79, 2959 (1997).

[42] S. E. Harris and L. V. Hau, Phys. Rev. Lett. 82, 4611 (1999).

[43] M. T. Johnsson and M. Fleischhauer, Phys. Rev. A 66, 043808 (2002).

[44] C. A. olderbach, M. Stahler, S. Knappe, and R. Wynands, Appl. Phys. B 75, 605 (2002).

[45] D. Budker, D. F. Kimball, S. M. Rochester, V. V. Yashchuk, and M. Zolotorev, Phys. Rev. A 62, 043403 (2000).

[46] J. Kitching, S. Knappe, and L. Hollberg, Appl. Phys. Lett. 81, 553 (2002).

[47] M. M. erimaa, T. Lindvall, I. T. ittonen, and E. Ikonen, J. Opt. Soc. Am. B 20, 273 (2003).

[48] M. D. Lukin, M. Fleischhauer, A. S. Zibrov, H. G. Robinson, V. L. Velichansky, L. Hollberg, and M. O. Scully, Phys. Rev. Lett. 79, 2959 (1997).

[49] V. Sautenkov, M. Kash, V. Velichansky, and G. Welch, Laser Physics 9, 889 (1999).

[50] D. Budker, W. G. awlik, D. Kimball, S. Rochester, V. Yashchuk, and A. W. eis, Rev. Mod. Phys. 74, 1153 (2002).

[51] V. A. Sautenkov, M. D. Lukin, C. J. Bednar, I. Novikova, E. M. Ikhailov, M. Fleischhauer, V. L. Velichansky, G. R. Welch, and M. O. Scully, Phys. Rev. A 62, 023810 (2000).

[52] I. Novikova, A. B. M. atsko, and G. R. Welch, Opt. Lett. 26, 1016 (2001).

[53] G. Theobald, N. D. m. arco, V. G. iordano, and P. Cerez, Opt. Comm. 71, 256 (1989).

[54] B. Schuh, S. I. Kanorsky, A. W. eis, and T. W. Hansch, Opt. Comm. 100, 451 (1993).

[55] K. H. D. rake, W. Lange, and J. M. lynek, Opt. Comm. 66, 315 (1988).

[56] L. M. Barkov, D. A. M. elik-Pashaev, and M. S. Zolotorev, Opt. Comm. 70, 467 (1989).

[57] P. E. G. Baird, M. Irie, and T. D. W. olfenden, J. Phys. B 22, 1733 (1989).

[58] X. Chen, V. L. Telegdi, and A. W. eis, Opt. Comm. 78, 337 (1990).

[59] S. I. Kanorsky, A. W. eis, and J. Skalla, Appl. Phys. B 60, S165 (1995).

[60] D. Budker, V. Yashchuk, and M. Zolotorev, Phys. Rev. Lett. 81, 5788 (1998).

[61] D. Budker, D. J. Orlando, and V. Yashchuk, Am. J. Phys. 67, 584 (1999).

[62] A. S. Zibrov, I. Novikova, and A. B. M. atsko, Opt. Lett. 26, 1311 (2001).

[63] I. Novikova, A. B. M. atsko, and G. R. Welch, Appl. Phys. Lett. 81, 193 (2002).